Compact and Wideband Coupled-Line 3-dB Ring Hybrids

Coupled Line으로 구성된 작고 넓은 대역폭을 가지는 3-dB Ring Hybrids

Hee-Ran Ahn · Jungjoon Kim · Bumman Kim

안 희 란 · 김 정 준 · 김 범 만

Abstract

In this paper, two types of wideband 3-dB ring hybrids are compared and discussed to show the ring hybrid with a set of coupled-line sections better. However, the better one still has a realization problem that perfect matching can be achieved only with −3 dB coupling power. To solve the problem, a set of coupled-line sections with two shorts is synthesized using one- and two-port equivalent circuits and design equations are derived to have perfect matching, regardless of the coupling power. Based on the design equations, a modified Π-type of transmission-line equivalent circuit is newly suggested. It consists of coupled-line sections with two shorts and two open stubs and can be used to reduce a transmission-line section, especially when its electrical length is greater than π. Therefore, the $3\lambda/4$ transmission-line section of a conventional ring hybrid can be reduced to less than $\pi/2$. To verify the modified Π-type of transmission- line equivalent circuit, two kinds of simulations are carried out; one is fixing the electrical length of the coupled-line sections and the other fixing its coupling coefficient. The simulation results show that the bandwidths of resulting small transmission lines are strongly dependent on the coupling power. Using modified and conventional Π-types of transmission-line equivalent circuits, a small ring hybrid is built and named a compact wideband coupled-line ring hybrid, due to the fact that a set of coupled-line sections is included. One of compact ring hybrids is compared with a conventional ring hybrid and the compared results demonstrate that the bandwidth of a proposed compact ring hybrid is much wider, in spite of being more than three times smaller in size. To test the compact ring hybrids, a microstrip compact ring hybrid, whose total transmission-line length is 220°, is fabricated and measured. The measured power divisions(S_{21}, S_{41}, S_{23} and S_{43}) are −2.78 dB, −3.34 dB, −2.8 dB and −3.2 dB, respectively at a design center frequency of 2 GHz, matching and isolation less than −20 dB in more than 20 % fractional bandwidth.

요 약

두 종류의 넓은 대역폭을 갖는 ring hybrids(하나는 coupled line이 포함되어 있고, 다른 하나는 left-handed transmission line을 포함한 ring hybrids)가 비교되었으며, 비교 결과로부터 coupled line을 포함한 ring hybrid가 모든 면에서 우수한 특성을 가짐을 보여줬다. 그러나, coupled line을 포함한 ring hybrid는 −3 dB coupling power를 가질 경우에 한해서만이 perfect matching이 이루어지기 때문에, perfect matching을 갖는 coupled line ring hybrid는 2차원으로 구현하기는 거의 불가능하다. 이 문제를 해결하기 위해서 coupled line을 해석했고, 그 해석 결과로부터 coupling coefficient에 관계없이 어느 경우에도 perfect matching을 이룰 수 있는 설계 식을 유도했다. 이 설계식을 이용하여, transmission line의 길이가 π보다 큰 경우에도 적용될 수 있는 크기를 줄이기 위한 새로

포항공과대학교 전자전기공학과(Dept. of Electronics and Electrical Engineering, Pohang University of Science and Technology(POSTECH))

· 논 문 번 호 : 20080523-09S
· 수정완료일자 : 2008년 7월 25일

운 형태의 transmission line 등가회로를 제시했다. 이 새로운 형태의 transmission line의 등가회로를 이용하면 기존의 ring hybrid의 3 λ/4의 transmission line을 줄이는 데 사용할 수 있기 때문에 ring hybrid의 크기를 더욱 줄이는 데 장점이 될 수 있다. 이 등가회로를 증명하기 위해서, coupling power를 고정하고 또는 transmission line의 길이를 고정하는 2가지 형태의 simulation을 하였으며, 대역폭은 coupled line의 coupling power에 직접적인 상관 관계가 있음을 보였다. 기존의 등가회로와 새로운 형태의 등가회로를 이용하여, 작고 넓은 대역폭을 가지는 ring hybrid를 제시하였다. 새로 제시된 ring hybrid를 이용하여, 기존의 ring hybrid와 비교하였다. 비교 결과로부터, 본 논문에서 제시한 ring hybrid의 전체 ring 둘레가 1/3보다 더 작음에도 불구하고, 대역폭이 훨씬 넓음을 보여줬다. 작고 넓은 대역폭을 가지는 ring hybrid를 측정했으며, 측정 결과는 −2.78 dB, −3.34 dB, −2.8 dB, −3.2 dB의 power division 특성을 보여줬으며, matching과 isolation은 20 % 이상의 대역폭에서 −20 dB보다 좋은 특성을 보여줬다.

Key words : Compact Wideband Coupled-Line Ring Hybrids, Modified Π-Type of Transmission-Line Equivalent Circuit, a Set of Coupled-Lines with Two Shorts, Wideband Coupled-Line Ring Hybrids

Ⅰ. Introduction

The ring hybrids are indispensable and fundamental components which can be used for various applications such as balanced amplifiers, balanced mixers, multipliers, phase shifters and attenuators, power amplifiers, antenna feeding networks and so on. Since the first ring hybrid was introduced in 1947 by Tyrrel [1], a number of engineers discussed performance and realization of the ring hybrids[2],[3]. However, the conventional ring hybrid, consisting of only transmission-line sections, is inherently of narrow bandwidth and large in size. To overcome this disadvantage, S. March[4] suggested a wideband ring hybrid having a set of coupled-line sections but the problem still remained: perfect matching can be achieved only with −3 dB coupling coefficient. The ring hybrids suggested by S. March will be named coupled-line ring hybrids, hereafter. However, the coupled-line sections with −3 dB coupling coefficient can not be easily realized and many efforts have been done to solve this problem; using broadside[5] and vertical coupling[6], uniplanar structures[7]~[10], left-handed transmission-line section[11] and so on. However, the left-handed transmission-line section should be realized with lumped elements, multisections are used for wideband performance[6], and in any case where the coupled-line sections are used, −3 dB coupling is not changed[4],[5],[7]~[10] for perfect matching.

To get compact ring hybrids, two design methods have been applied; using arbitrary transmission-line sections[7],[12],[13] and transmission-line equivalent circuits [14],[15]. However the compact ring hybrids designed by the first method are perfectly matched at a frequency where transmission-line sections become 90°. Therefore, size reduction effect can not be expected. For the second method, lumped-element[16]~[19], Π-type[14],[15] or T-type of transmission-line equivalent circuits are used. However, in the T-type of equivalent circuit, the characteristic impedance of transmission-line section becomes very high with small size reduction. Using the lumped-element equivalent circuit, the bandwidth of resulting small transmission lines is very small. The conventional Π-type of transmission-line equivalent circuit can be used only when the transmission-line length is less than π.

In this paper, a wideband coupled-line ring hybrid is compared with a ring hybrid having a left-handed transmission-line section[11] and the compared results show that the coupled-line ring hybrid is better in any case. The coupled-line sections of the ring hybrid is a kind of impedance transformer[7],[17] and can be obtained from a four-port directional coupler for impedance transforming, very recently introduced[20],[21]. However, in this case, perfect matching can be achieved only with −3 dB coupling. To have perfect matching with any coupling coefficient, the coupled-line sections with two shorts are synthesized using one- and two-port equivalent circuits and design equations are derived to design and fabricate the wideband coupled-line ring hybrids in planar structure, without any restriction of coupling power.

Also, to reduce the ring hybrid size more, modified Π-type of transmission-line equivalent circuit is newly proposed based on the design equations of the coupled-line sections with two shorts. The modified equivalent circuit can be used for any transmission-line section whose electrical length is greater than π and therefore the $3\lambda/4$ transmission-line section of a ring hybrid can be reduced more. Using both modified and conventional Π-types of equivalent circuits, compact wideband coupled-line ring hybrids are newly constructed and one of them is compared with the conventional ring hybrid in terms of power division. The compared results demonstrate that the compact ring hybrid proposed in this paper shows more bandwidth in spite of being three times smaller in size. To test the compact ring hybrids, one microstrip ring hybrid is fabricated and measured. The measured power divisions(S_{21}, S_{41}, S_{23} and S_{43}) are −2.78 dB, −3.34 dB, −2.8 dB and −3.2 dB, respectively at a design center frequency of 2 GHz and matching and isolation less than −20 dB in more than 20 % fractional bandwidth.

This paper is constructed with six sections. Section I gives brief introduction of conventional wideband ring hybrids and contents of this paper. Section II compares conventional wideband ring hybrids to know which one has better performance and which problem the better one has. In section Ⅲ, coupled-line sections with two shorts are synthesized to solve the problem, that is, to realize them without any restriction of coupling power. In section Ⅳ, using the design equations of the coupled-line sections with two shorts, wideband coupled-line ring hybrids are simulated to show perfect matching can be achieved, independently of coupling power. Then, to reduce the ring hybrid size more, a modified Π-type of transmission-line equivalent circuit is newly proposed and how to get compact wideband coupled-line ring hybrids is discussed in section Ⅴ. Finally, this paper concludes with section Ⅵ.

Ⅱ. Conventional Ring Hybrids

2-1 Conventional Ring Hybrids

Three 3-dB conventional ring hybrids terminated in equal impedances Z_0 are depicted in Fig. 1. The conventional ring hybrid in Fig. 1(a), consisting of three $\lambda/4$ transmission-line sections and one $3\lambda/4$ transmission-line section, is inherently of narrow bandwidth and large in size. The shortcoming is mainly due to that the bandwidth, where $\lambda/4$ and $3\lambda/4$ transmission-line sections have 180° phase difference, is very narrow. To increase the bandwidth, that is, to have 180° phase difference in wider bandwidth, the $3\lambda/4$ transmission-line section is replaced by a set of coupled-line sections with two shorts or a left-handed transmission-line section, as described in Fig. 1(b) and (c), respectively. Because of the reason, the ring hybrid in Fig. 1(b) is named "a coupled-line ring hybrid" and that in Fig. 1(c)

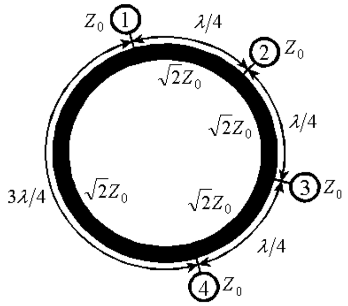

(a) A ring hybrid with a $3\lambda/4$ transmission-line section between ports ① and ④

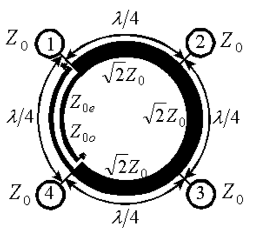

(b) A coupled-line ring hybrid

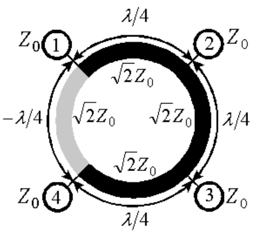

(c) A left-handed ring hybrid

Fig. 1. Conventional ring hybrids.

"a left-handed ring hybrid." However, the two ring hybrids have realization problems; in the coupled-line ring hybrid in Fig. 1(b), the perfect matching can be achieved only with −3 dB coupling coefficient, and the left-handed transmission-line section may be realized only with lumped-elements which may cause unwanted frequency performance.

2-2 Conventional Wideband Ring Hybrids

To compare the two ring hybrids in Fig. 1(b) and (c), the two are simulated at a center frequency of 1 GHz and the simulation results are plotted in Fig. 2. In this case, the even- and odd-mode impedances of the coupled-line sections in Fig. 1(b) are 171.4 Ω and 29.3 Ω, respectively when Z_0 is 50 Ω[4],[5]. The power excited at port ① or ③ in Fig. 1 is divided equally between ports ② and ④ and isolated from port ③ or ①, respectively. The divided waves are in phase or out of phase, depending on the input port chosen. Considering these points, the ratios of S_{21} to S_{41} and S_{23} to S_{43}, and phase differences of $|\angle S_{21}-\angle S_{41}|$ and $|\angle S_{23}-\angle S_{43}|$ are plotted in Fig. 2 where solid lines indicate the frequency responses of the coupled-line ring hybrid and the dotted ones are those of the left-handed ring hybrid.

In 100 % fractional bandwidth, S_{21}/S_{41} of the coupled-line ring hybrid exists from 0 dB to 0.567 dB and S_{23}/S_{43} from 0 dB to 0.724 dB as shown in Fig. 2(a). On the other hand, in the left-handed ring hybrid, S_{21}/S_{41} exists between 0 dB and 0.9 dB and S_{23}/S_{43} from −0.9 dB to 0 dB as displayed in Fig. 2(a). The less power division ratios, the better. Therefore, the coupled-line ring hybrid is better than the left-handed ring hybrid in terms of power divisions.

In phase responses in Fig. 2(b), out-of-phase response, $|\angle S_{21}-\angle S_{41}|$ of the coupled-line ring hybrid exists between 170.4° and 188.3° while that of the left-handed ring hybrid between 137.6° and 228.3°. In Fig. 2(c), in-phase response, $|\angle S_{23}-\angle S_{43}|$ of the coupled-line ring hybrid is between 0° and 9.4° and that of the left-handed ring hybrid between 0° and 25.66°. Since the ideal phase differences of $|\angle S_{21}-\angle S_{41}|$ and $|\angle S_{23}-\angle S_{43}|$ are equal to 180° and 0°, respectively, the coupled-line ring hybrid is much better than the left-handed ring hybrid in terms of phase response. Exact simulation results are written in Table 1 where the coupled-line ring hybrid show the better performance than those of the left-handed ring hybrid, in every point.

Table 1. Simulation results within a 100 % fractional bandwidth(CPL and LH stand for coupled-line and left-handed ring hybrids, respectively).

	dB(S_{21}/S_{41})	dB(S_{23}/S_{43})
CPL	0～0.567 dB	0～0.724 dB
LH	0～0.902 dB	−0.902～0 dB
	$\lvert\angle S_{21}-\angle S_{41}\rvert$	$\lvert\angle S_{23}-\angle S_{43}\rvert$
CPL	170.4～188.3°	0～9.4°
LH	137.6～228.3°	0～25.66°

Even though the performance of the coupled-line ring hybrid is much better than that of the left-handed ring hybrid in every point, how to realize high even-mode impedance of 171.4 Ω and low odd-mode impedance of 29.3 Ω in microstrip technology is a big problem. To solve the problem, the coupled-line sections with two shorts connected between ports ① and ④ in Fig. 1(b) will be discussed in more detail.

Ⅲ. Coupled Lines with Two Shorts

3-1 Coupled Lines with Two Shorts

As discussed in the literatures[7],[17], the coupled-line sections with two shorts connected between ports ① and ④ in Fig. 1(b) is used as an impedance transformer to transform $2Z_0$ into Z_0, when power is fed into port ①. The coupled-line sections with two shorts may be derived from a four-port impedance transforming directional coupler discussed in the literatures[20],[21]. The directional coupler for an impedance transformer and a two-port coupled-line sections with two shorts are depicted in Fig. 3(a) and (b), respectively where an input-im-

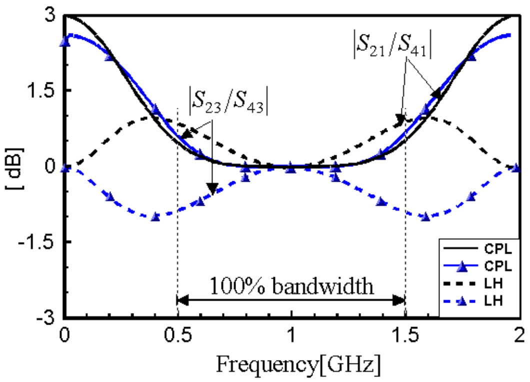

(a) Power division ratios

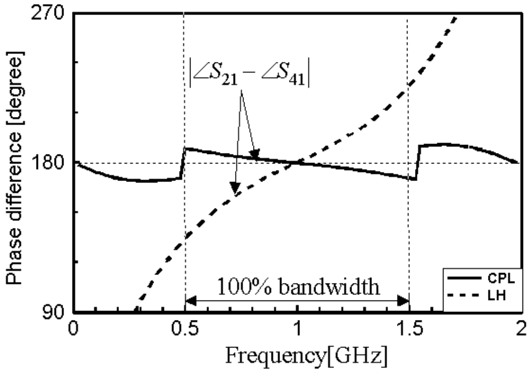

(b) Out-of-phase response

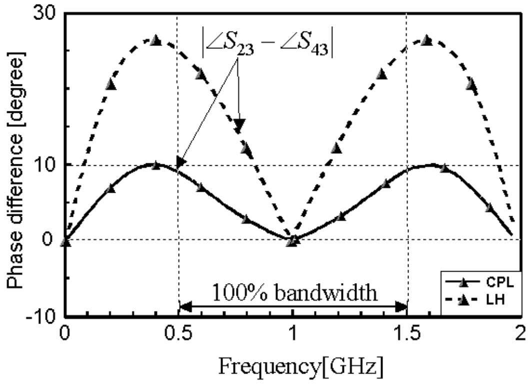

(c) In-phase response

Fig. 2. Two wideband ring hybrids are compared and CPL and LH indicate coupled-line and left-handed ring hybrids, respectively.

pedance Z_{in}, looking into the coupled-line sections terminated in Z_L at port ②, is indicated in Fig. 3(b).

When $\Theta=\pi/2$ in Fig. 3(a), the power excited at port ① is coupled to port ② with a certain coupling power and the remainder of the input power is delivered to port ④. Theoretically, no power is delivered to port ③, which is called an isolated port. In this case, the even- and odd-mode impedances[20],[21] are

$$Z_{0e}=\sqrt{Z_r Z_L}\sqrt{\frac{1+C}{1-C}} \tag{1a}$$

$$Z_{0o}=\sqrt{Z_r Z_L}\sqrt{\frac{1-C}{1+C}} \tag{1b}$$

where C is a coupling coefficient.

Terminating ports ② and ④ in Fig. 3(a) in two shorts results in the coupled-line sections with two shorts in Fig. 3(b). Applying the short boundary condition gives its admittance matrix as

$$[Y]=\begin{bmatrix} -j\dfrac{Y_{0e}+Y_{0o}}{2}\cot\Theta & -j\dfrac{Y_{0o}-Y_{0e}}{2}\csc\Theta \\ -j\dfrac{Y_{0o}-Y_{0e}}{2}\csc\Theta & -j\dfrac{Y_{0e}+Y_{0o}}{2}\cot\Theta \end{bmatrix} \tag{2}$$

where $Y_{0e}=1/Z_{0e}$, $Y_{0o}=1/Z_{0o}$ and a pure TEM(transverse electromagnetic) propagation is assumed.

Based on the admittance matrix in (2), the scattering parameters of coupled-line sections in Fig. 3(b) are derived as

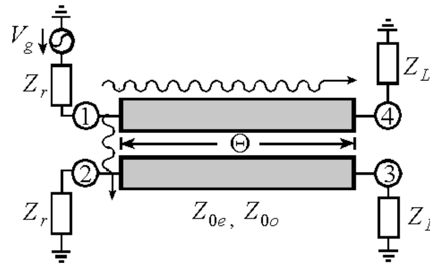

(a) Directional coupler

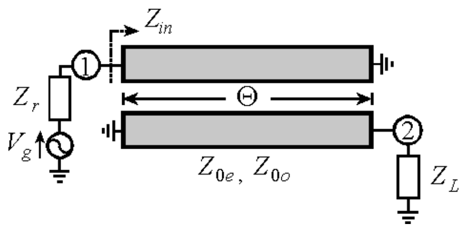

(b) Coupled-line sections with two shorts

Fig. 3. Impedance transforming directional coupler and coupled-line sections with two shorts.

$$S_{11} = \frac{1}{D}[(Y_{0o} - Y_{0e})^2 \sec^2\Theta - (Y_{0e} + Y_{0o})^2 - 4Y_r Y_L \tan^2\Theta - j2(Y_{0o} + Y_{0e})(Y_L - Y_r)\tan\Theta] \quad (3a)$$

$$S_{22} = \frac{1}{D}[(Y_{0o} - Y_{0e})^2 \sec^2\Theta - (Y_{0e} + Y_{0o})^2 - 4Y_r Y_L \tan^2\Theta + j2(Y_{0o} + Y_{0e})(Y_L - Y_r)\tan\Theta] \quad (3b)$$

$$S_{21} = \frac{1}{D}[-j4Y_r(Y_{0o} - Y_{0e})\sin\Theta\sec^2\Theta] \quad (3c)$$

where $D = (Y_{0e} + Y_{0o})^2 - (Y_{0o} - Y_{0e})^2 \sec^2\Theta - 4Y_r Y_L \tan^2\Theta + j2(Y_{0e} + Y_{0o})(Y_r + Y_L)\tan\Theta$,

$Y_r = 1/Z_r$ and $Y_L = 1/Z_L$.

Using the calculation results in (3), the coupled-line sections with two shorts were simulated by use of a mathematical software Matlab 6.1 and simulation results are plotted in Fig. 4 where the termination impedances, Z_r and Z_L are 50 Ω and 100 Ω, respectively. Depending on the coupling coefficients, coupling characteristics are classified as critical coupling($C=-3$ dB), over coupling($C>-3$ dB) and under coupling($C<-3$ dB)[22]. Fig. 4 shows that perfect matching appears only with the critical coupling, and that ripples with no perfect matching exist in the over coupling case. The power excited at port ① in Fig. 3(b) is transmitted into port ②, and how much power can be transmitted is dependent on the coupling structure. In order that the perfect matching at a design center frequency can be achieved regardless of the coupling coefficient, design equations will be derived using one- and two-port equivalent circuits.

3-2 One-Port Equivalent Parallel Resonant Circuit

How much power excited at port ① in Fig. 3(b) can be transmitted into port ② is dependent on the coupling structure. So, the coupled-line sections terminated in Z_L in Fig. 3(b) may be equivalent to a one-port parallel resonant circuit[22] as described in Fig. 5 where input impedance and input reference impedance Z_{in} and Z_r are indicated.

The input impedance Z_{in}[23] in Fig. 3(b) and Fig. 5 is calculated by use of the following equation;

$$Z_{in} = [Y_{in}]^{-1} = \left[Y_{11} - \frac{Y_{12}Y_{21}}{Y_{22} + Y_L} \right]^{-1} \quad (4)$$

which gives frequency dependent R_o, L_o and C_o in Fig. 5 as follows;

$$R_o = \frac{Y_L(1 - C^2) + Y_r \cot^2\Theta}{Y_r Y_L C^2 \csc^2\Theta} \quad (5a)$$

for $\cot\Theta \geq 0$

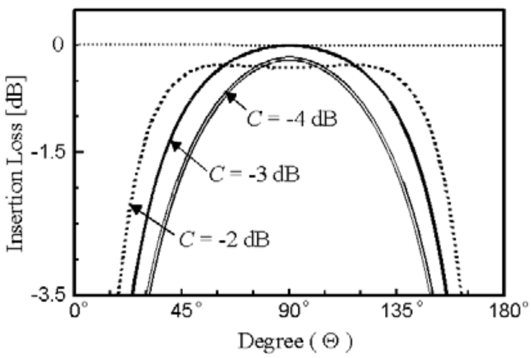

(a) Insertion loss

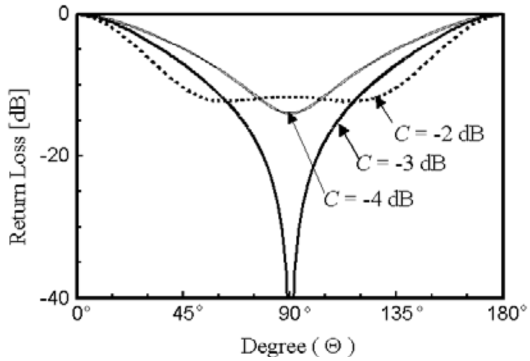

(b) Return loss

Fig. 4. Simulation results of the coupled-line sections with two shorts(C is coupling coefficient).

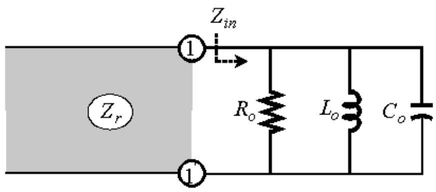

Fig. 5. One-port equivalent parallel resonant circuit.

$$\omega C_o = C^2\left[\sqrt{\frac{Y_rY_L}{1-C^2}}\right]^3 \frac{\cot\Theta}{\sin^2\Theta} \tag{5b}$$

$$\omega L_o = \frac{\left(\sqrt{1-C^2}\right)^3}{Y_L\sqrt{Y_rY_L}\cot\Theta[Y_r\cot^2\Theta + Y_L(1-C^2)]} \tag{5c}$$

for $\cot\Theta < 0$

$$\omega C_o = \frac{Y_L\sqrt{Y_rY_L}\cot\Theta[Y_r\cot^2\Theta + Y_L(1-C^2)]}{\left(\sqrt{1-C^2}\right)^3} \tag{5d}$$

$$\omega L_o = \left[\sqrt{\frac{1-C^2}{Y_rY_L}}\right]^3 \frac{\sin^2\Theta}{C^2\cot\Theta} \tag{5e}$$

The input impedance Z_{in} may be displayed on an impedance Smith chart and Fig. 6 illustrates coupling to a parallel resonant circuit. In this case, Z_r =50 Ω and Z_L =100 Ω in Fig. 3(b) are fixed, and coupling coefficient and electrical length Θ are varied as shown in Fig. 6. The input impedance loci cut the real axis two times, and when $\Theta = \pi/2$, the input impedance normalized to Z_r is exactly unity with the critical coupling but the two others are more or less than unity. It means that a perfect matching appears only with the critical coupling; these results coincide with those in Fig. 4. For any set of coupled-line sections with two shorts in Fig. 3(b) to have perfect matching, regardless

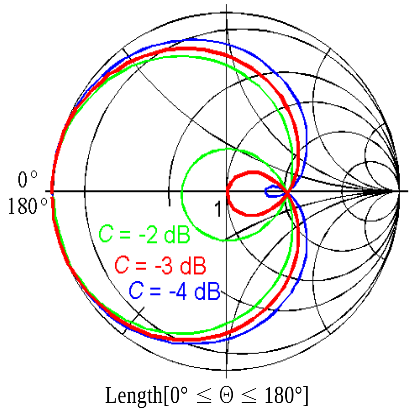

Fig. 6. Input impedances are illustrated on an impedance Smith chart depending over, critical and under coupling.

of the coupling coefficient, the even- and odd-mode impedances need to be modified in such a manner that the over- coupled input impedances are increased and those of the under coupled ones are decreased. When $\Theta = \pi/2$ in (5), only R_o appears and its value is

$$R_o = Z_r\frac{1-C^2}{C^2} \tag{6}$$

From (6), R_o is Z_r when $C = 1/\sqrt{2}$ (critical coupling), which agrees with the simulation results in Figs. 4 and 6. For the coupled-line sections to be perfectly matched at a design center frequency with any coupling coefficient, the even- and odd-mode impedances should be modified so that the value of R_o is always Z_r, regardless of the coupling coefficient. The Z_r in (6) comes from the even- and odd-mode impedances in (1) and can be modified to have a constant value of input impedance. The solution for this is to replace Z_r in (1) by $Z_r[C^2/(1-C^2)]$.

In such a manner, the modified even- and odd-mode impedances Z_{0e}^m and Z_{0o}^m are derived as

$$Z_{0e}^m = \frac{C}{1-C}\sqrt{Z_rZ_L} \tag{7a}$$

$$Z_{0o}^m = \frac{C}{1+C}\sqrt{Z_rZ_L} \tag{7b}$$

With Z_{0e}^m and Z_{0o}^m, the input impedance Z_{in} always becomes $R_o = Z_r$ at resonant frequency, that is, at a center frequency, regardless the coupling coefficient.

3-3 Two-Port Equivalent Circuit

A set of coupled-line sections with electrical length Θ and termination admittances Y_r and Y_L in Fig. 3(b) may be equivalent to a circuit, consisting of a transmission-line section with electrical length $\pi+\Theta$ and two stubs as depicted in Fig. 7 where the characteristic admittances of transmission-line section and stubs are $(Y_{0o}-Y_{0e})/2$ and Y_{0e}, respectively. When $\Theta=\pi/2$, only the transmission-line section is connected between the two termination admittances and should be a quarter wave admittance transformer. Therefore, its characteristic admittance is a geometric mean value of the two

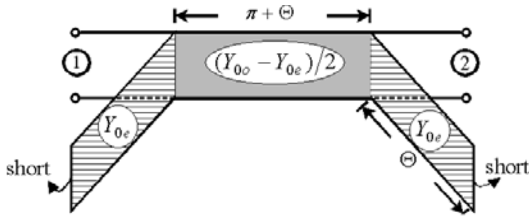

Fig. 7. Two-port equivalent circuit of coupled-line sections with two shorts.

termination admittances and related with the coupling coefficients[20],[21]. So, the relative relations are given as

$$\frac{Y_{0o} - Y_{0e}}{2} = \sqrt{Y_r Y_L} \tag{8a}$$

$$Y_{0o} = \frac{1+C}{1-C} Y_{0e} \tag{8b}$$

The even- and odd-mode admittances satisfying (8) are different from the original ones in (1) and calculated as

$$Y_{0e}^m = \frac{1-C}{C} \sqrt{Y_r Y_L} \tag{9a}$$

$$Y_{0o}^m = \frac{1+C}{C} \sqrt{Y_r Y_L} \tag{9b}$$

which are the same as those in (7).

As shown in the equivalent circuit in Fig. 7, the transmission-line section can considered as a circuit where a transmission-line section with Θ is connected with a frequency independent 180° phase shifter. Therefore, $\lambda/4$ transmission-line section and $\lambda/4$ coupled-line sections in Fig. 1 can have 180° phase difference in wider frequency band. That is the reason the coupled-line ring hybrid in Fig. 1(b) can have wideband performance.

3-4 Coupled-Line Section Measurements

To verify the design equations in (7) and (9), a microstrip coupled-line sections with two shorts terminated in 100 Ω and 50 Ω was fabricated on a substrate(H =0.76 mm and ε_r =3.4) and tested at a center frequency of 2 GHz. Table 2 gives Z_{0e}^m and Z_{0o}^m depending on the coupling coefficient where the even- and odd-mode impedances with −3 dB coupling coefficient are 171.4 Ω and 29.3 Ω, respectively, which are almost impossible to realize with two-dimensional microstrip lines.

For the measurement, a microstrip coupled-line sections with $C = -7$ dB was fabricated and its even- and odd-mode impedances are Z_{0e}^m =57.1 Ω and Z_{0o}^m =21.8 Ω as given in Table 2. The even- and odd-mode impedances required above can be realized without any problem using a stand PCB(printed circuit board) technology but an easy method, with which the odd-mode impedance can be fabricated in a school, will be introduced.

The even-mode impedance of 57.1 Ω can be realized without any problem, but the odd-mode impedance is somewhat difficult because the given substrate has a low dielectric constant. Therefore, a three-dimensional structure or a set of three coupled-line sections is needed to get the odd-mode impedance. In our case, the three-dimensional structure[24] was used.

If a TEM propagation of two coupled transmission lines is assumed, then the characteristics of coupled transmission lines can be completely determined from capacitances and propagation velocities on the transmission lines. Two-dimensional capacitance equivalent network of a pair of coupled transmission lines is shown in Fig. 8(a) where C_{12} represents the capacitance per unit length between the two conductor lines in the absence of the ground conductor, while C_{11} and C_{22} denote the capacitances per unit length between one conductor and ground, in the absence of the other conductor line. If the coupled transmission lines are identical in size, then $C_{11} = C_{22}$. For the even-mode excitation, no current flows between the two trans-

Table 2. Even and odd-mod impedances with Z_r = 100 Ω and Z_L =50 Ω.

C [dB]	−3	−5	−7	−9	−11
Z_{0e}^m [Ω]	171.4	90.9	57.1	38.9	27.8
Z_{0o}^m [Ω]	29.3	25.5	21.8	18.5	15.5

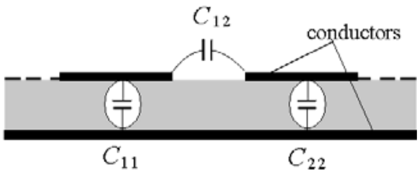

(a) Side view of a two-dimensional equivalent capacitance network

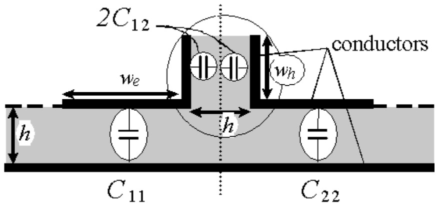

(b) Side view of a three-dimensional equivalent capacitance network

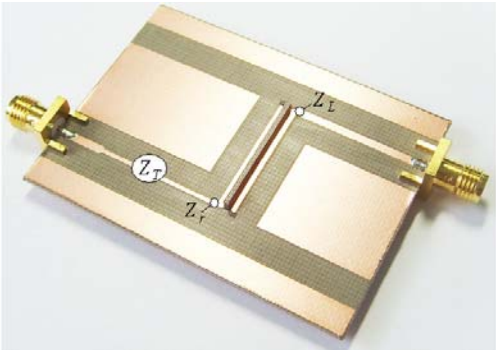

(c) Fabricated microstrip coupled lines with two shorts

Fig. 8. A microstrip coupled lines with two shorts terminated in 100 Ω and 50 Ω and general coupled lines.

mission lines, which leads to $C_{12}=0$. The resulting capacitance of either line to ground is $C_e=C_{11}=C_{22}$ and its even-mode impedance Z_{0e} is $\sqrt{\varepsilon\mu}/C_e$, where ε and μ are permittivity and permeability of a substrate, respectively. For the odd-mode excitation, the electric field lines have an odd symmetry about the center line and a voltage null exists between the two transmission lines. So, its resulting capacitance of either line to ground is $C_o=C_{11}+2C_{12}$ and the odd-mode impedance Z_{0o} is $\sqrt{\varepsilon\mu}/C_o$. As mentioned above, the even- and odd-mode impedances are proportional to the square root of a substrate dielectric constant and if the odd-mode capacitance is too big, that is, a tight coupling, the odd-mode impedance is not easy to realize.

To realize the low odd-mode impedance with three-dimensional structure as shown in Fig. 8(b), a pair of coupled transmission lines, with which only a required even-mode impedance can be realized, is first fabricated with a space of h, here h is an assumed thickness of a given substrate. Then, the width w_h of a conductor vertically constructed in Fig. 8(b) is determined to have the required odd-mode impedance. In this case, the even-mode impedance is connected in parallel with the impedance produced by the vertical conductor.

Design data for the microstrip coupled-line sections with $C=-7$ dB are given in Table 3 where Z_T is a characteristic impedance of a quarter wave impedance transformer to transform 100 Ω into 50 Ω. For the given substrate, a pair of coupled transmission lines is first realized, fixing its space at the thickness of the given substrate in order that only the even-mode impedance of 57.1 Ω can be obtained. For the odd-mode excitation, since a voltage null exist between two coupled transmission lines, the even-mode impedance of 57.1 Ω is connected in parallel with an impedance produced between a vertically constructed conductor and the voltage null between the two coupled lines. This results in the required odd-mode impedance $Z_{0o}{}^{m}=21.8$ Ω. Therefore, the impedance produced from the vertical conductor is 35.3 Ω, symbolized as a marked Z_v in Table 3. The characteristic impedance of Z_v is easily realized using a commercial simulation tool but an important point is its effective thickness is half of the

Table 3. Fabrication data for a microstrip coupled line with two shorts.

<table>
<tr><td colspan="2">$Z_r=100$ Ω, $Z_L=50$ Ω, $Z_T=70.71$ Ω,
substrate(H=0.76 mm and $\varepsilon_r=3.4$)</td></tr>
<tr><td>$Z_{0e}{}^{m}=57.1$ Ω</td><td>$w_e=1.34$ mm, $\ell=22.9$ mm,
$s=0.76$ mm</td></tr>
<tr><td>$Z_{0o}{}^{m}=21.8$ Ω</td><td>$Z_v=35.3$ Ω $\rightarrow$
$w_h=1.407$ mm, $\ell=22.9$ mm</td></tr>
<tr><td colspan="2">Z_T : w=0.895 mm, ℓ=23.28 mm
50 Ω:w=1.678 mm</td></tr>
</table>

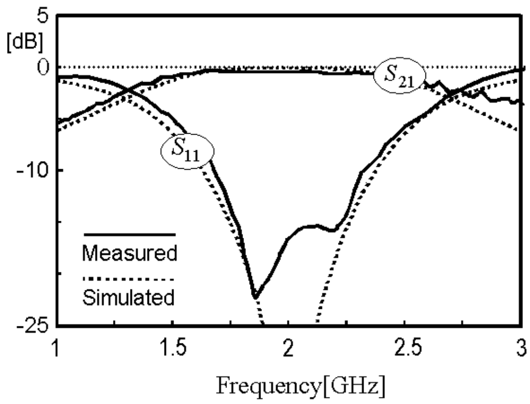

Fig. 9. Results measured and simulated are compared.

given substrate thickness. In this way, the microstip coupled transmission lines were fabricated as shown in Fig. 8(c). Fig. 9 compares the measured and predicted results and they show good agreement between them.

Ⅳ. Wideband Coupled-Line Hybrids

Using the analyzed coupled lines, wideband coupled-line ring hybrids can be realized without any restriction of coupling coefficient. As mentioned before, the coupled-line sections between ports ① and ④ in Fig. 1(b) is a kind of impedance transformer to transform 100 Ω into 50 Ω, when Z_0 =50 Ω. Therefore, the data given in Table 2 may be used and several coupled-line ring hybrids are compared in terms of port ① excitation. The compared results are plotted in Fig. 10 where perfect matching at a center frequency is achieved regardless of the coupling coefficients and the bandwidth is proportional to the coupling power.

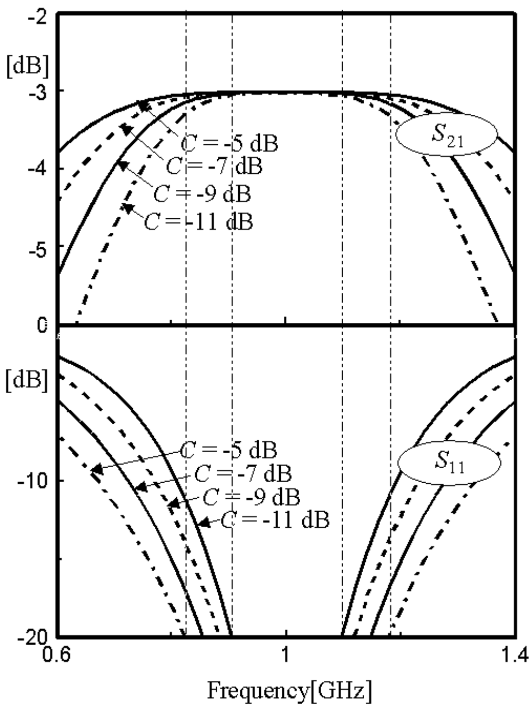

Fig. 10. Several coupled-line ring hybrids.

Ⅴ. Compact Wideband Coupled-Line Ring Hybrids

5-1 Small Transmission Lines

The coupled-line and left-handed ring hybrids in Fig. 1(b) and (c) are somewhat smaller than the conventional ring hybrids in Fig. 1(a) but they are still large in size. To reduce the size of ring hybrids, transmission-line sections are required to be reduced. For this purpose, conventional Π-type of transmission-line equivalent circuit was suggested but it can be used only when its electrical length is less than π. To reduce the size of ring hybrids more, modified Π-type of transmission-line equivalent circuit is newly suggested. It can be used to reduce the 3λ/4 transmission-line section of a conventional ring hybrids to less than $\pi/2$. Transmission-line sections with characteristic impedance Z_0, their conventional and modified Π-types of transmission-line equivalent circuits are depicted in Fig. 11 where Θ and Θ_s are less than π and $\pi/2$, respectively. Therefore, the equivalent circuit in Fig. 11(b) is used when $\Theta \le \pi$ and that consisting of coupled-line sections in Fig. 11(d) for transmission-line sections with more than π.

The even- and odd-mode impedances Z_{0e}^s and Z_{0o}^s in Fig. 11 are computed, applying $Z_r = Z_L$ in Fig. 3(b), (7) and (9) and the relations between Θ, Z_0, Z_s, Θ_s, Y_{op}, Θ_{op}, Z_{0e}^s, Z_{0o}^s, Y_{cop} and Θ_{cop} in Fig. 11 are derived as

$$Z_s = Z_0 \frac{\sin\Theta}{\sin\Theta_s} \tag{10a}$$

$$Y_{op}\tan\Theta_{op} = Y_0 \frac{\cos\Theta_s - \cos\Theta}{\sin\Theta} \tag{10b}$$

$$Z_{0e}^{s} = Z_0 \frac{\sin\Theta}{\sin\Theta_s}\frac{C}{1-C} \tag{10c}$$

$$Z_{0o}^{s} = Z_0 \frac{\sin\Theta}{\sin\Theta_s}\frac{C}{1+C} \tag{10d}$$

$$Y_{cop}\tan\Theta_{cop} = \frac{Y_0}{\sin\Theta}\left(\frac{\cos\Theta_s - C\cos\Theta}{C}\right) \tag{10e}$$

where $Y_0 = 1/Z_0$ and C is coupling coefficient.

When $Z_0 = 70.71$ Ω and $\Theta = \pi/2$ in Fig. 11(c), it is equal to the 3/ λ4 transmission-line section between

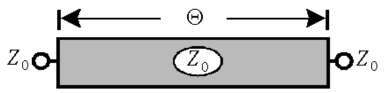

(a) A transmission-line section with $\Theta < \pi$

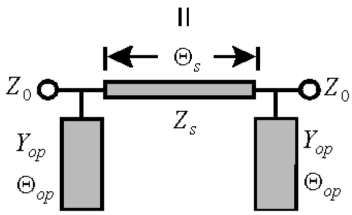

(b) A conventional Π-type of transmission-line equivalent circuit with $\Theta_s \le \pi/2$

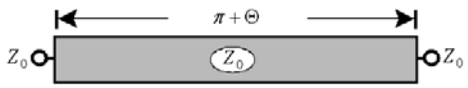

(c) A transmission-line section with electrical length more than π

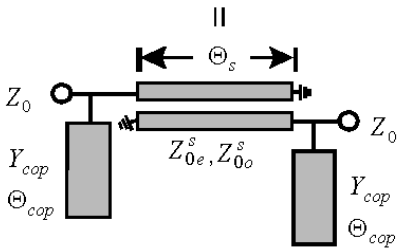

(d) A modified Π-type of transmission-line equivalent circuit with $\Theta_s \le \pi/2$

Fig. 11. Transmission-line sections and their equivalent circuits.

Table 4. Design data for small transmission lines.

Θ_s =60°, Θ_{cop} =30°			
C [dB]	−5	−7	−9
Z_{0e}^{s}	104.9	65.9	44.9
Z_{0o}^{s}	29.4	25.2	21.4
Z_{cop}	45.9	36.5	29

Table 5. Design data for small transmission lines.

C = −7 dB, Θ_{cop} =30°			
Θ_s	40°	50°	60°
Z_{0e}^{s}	88.8	74.5	65.9
Z_{0o}^{s}	33.97	28.5	25.2
Z_{cop}	23.8	28.4	36.5

ports ① and ④ of the conventional ring hybrid in Fig. 1(a). Based on the equations in (10) and (11), when Z_0 =70.71 Ω, $\Theta = \pi/2$, with Θ_{cop} =30° and Θ_s =60° fixed, Z_{0e}^{s}, Z_{0o}^{s} and Z_{cop} are calculated as the coupling coefficients are varied and the calculation results are given in Table 4. When Z_0 =70.71 Ω, $\Theta = \pi/2$, with Θ_{cop} =30° and C =−7 dB fixed, Z_{0e}^{s} , Z_{0o}^{s} and Z_{cop} are calculated as the electrical lengths of Θ_s are varied and the calculation results are written in Table 5. Based on Tables Ⅳ and Ⅴ, several small transmission-line sections in Fig. 11(d) are simulated and the simulation results are plotted in Fig. 12 where one can know that the more coupling power gives more bandwidth but the bandwidth is not strongly dependent on the electrical length Θ_s when the coupling coefficient is fixed.

5-2 Compact Wideband Coupled-Line Ring Hybrids

Using the relations in Fig. 11, a compact wideband coupled-line ring hybrid can be built as depicted in Fig. 13 where the following relations hold;

$$Y_{r1}\tan\Theta_{r1} = 2Y_{op}\tan\Theta_{op} \tag{11a}$$

$$Y_{r2}\tan\Theta_{r2} = Y_{op}\tan\Theta_{op} + Y_{cop}\tan\Theta_{cop} \tag{11b}$$

where $Y_{r1} = 1/Z_{r1}$ and $Y_{r2} = 1/Z_{r2}$.

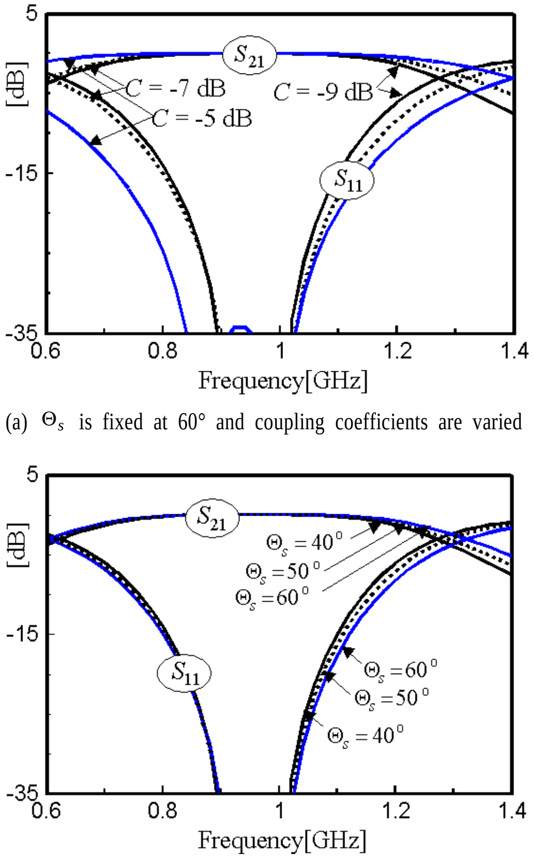

(a) Θ_s is fixed at 60° and coupling coefficients are varied

(b) Coupling C is fixed at −7 dB and Θ_s is varied

Fig. 12. Simulation results of small transmission-line sections consisting of coupled lines.

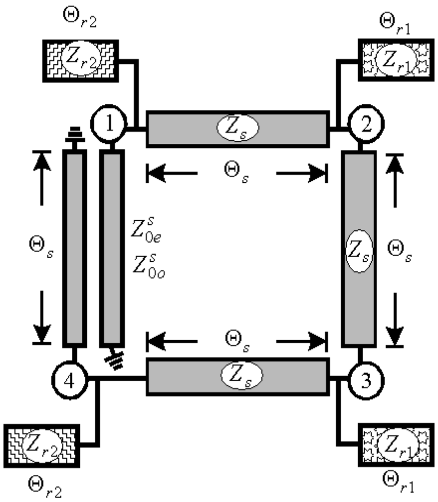

Fig. 13. Proposed compact wideband coupled-line ring hybrid.

The compact wideband coupled-line ring hybrids are designed at a center frequency of 1 GHz using Table 6 and compared with a conventional ring hybrid in Fig. 1(a). The compared simulation results are plotted in Fig. 14 where only power division frequency response is plotted. In this case, the total transmission-line length of the compact wideband coupled-line ring hybrids is 160°, whereas that of the conventional one is 540°. From the compared results of the power divisions, the proposed compact ring hybrid shows wider bandwidth, in spite of being more than three times smaller in size. The compact ring hybrids are designed using the equations in (10), (11) and (12) and three types of data with variable Θ_s are listed in Tables 6～8 where Θ_s, Θ_{r1} and Θ_{r2} are fixed and coupling coefficient is varied from −5 dB to −11 dB.

Table 6. Design data of compact wideband coupled-line ring hybrids for $\Theta_s = 40°$.

$\Theta_s = 40°$				
$Z_s = 110\ \Omega$, $Z_{r1} = 38.73\ \Omega$, $\Theta_{r1} = 40°$				
C	−5 dB	−7 dB	−9 dB	−11 dB
Z_{0e}^s	141.3 Ω	88.8 Ω	60.5 Ω	43.2 Ω
Z_{0o}^s	39.6 Ω	33.97 Ω	28.8 Ω	24.2 Ω
Z_{r2}	27.9 Ω	23.9 Ω	20.3 Ω	17.0 Ω
Θ_{r2}	40°	40°	40°	40°

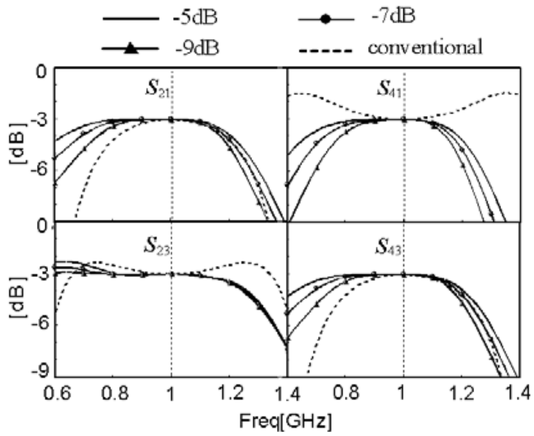

Fig. 14. Compared power division frequency responses.

Table 7. Design data of compact wideband coupled-line ring hybrids for $\Theta_s = 50°$.

$\Theta_s = 50°$				
$Z_s = 92.3\ \Omega$, $Z_{r1} = 65.5\ \Omega$, $\Theta_{r1} = 50°$				
C	−5 dB	−7 dB	−9 dB	−11 dB
Z_{0e}^s	118.6 Ω	74.5 Ω	50.8 Ω	36.2 Ω
Z_{0o}^s	33.2 Ω	28.5 Ω	24.2 Ω	20.3 Ω
Z_{r2}	47.2 Ω	40.5 Ω	34.3 Ω	28.8 Ω
Θ_{r2}	50°	50°	50°	50°

Table 8. Design data of compact wideband coupled-line ring hybrids for $\Theta_s = 60°$.

$\Theta_s = 60°$				
$Z_s = 81.6\ \Omega$, $Z_{r1} = 59.3\ \Omega$, $\Theta_{r1} = 40°$				
C	−5 dB	−7 dB	−9 dB	−11 dB
Z_{0e}^s	104.9 Ω	65.9 Ω	44.9 Ω	32.0 Ω
Z_{0o}^s	29.4 Ω	25.2 Ω	21.4 Ω	17.95 Ω
Z_{r2}	60.7 Ω	52.0 Ω	44.1 Ω	37.0 Ω
Θ_{r2}	50°	50°	50°	50°

5-3 Compact Coupled-Line Ring Hybrid Measurement

To test the compact ring hybrids, one microstrip ring hybrid was fabricated on a substrate(H =0.76 mm and ε_r =3.4) as shown in Fig. 15 where port numbers are indicated. Fabrication data are written in Table 9 where the transmission-line section of Θ_s is fixed at 55° and Z_{0e}^s and Z_{0o}^s are chosen as 64.21 Ω and 25.8 Ω, respectively.

The microstrip ring hybrid was tested at a center frequency of 2 GHz and the measured and predicted results are compared in Figs. 16 and 17 where measured frequency response is expressed as solid lines and dotted ones are prediction. When the power is excited at port ① in Fig. 15, the measured power division response is compared with simulation ones in Fig. 16(a) where the measured S_{21} and S_{41} show −3.34 dB and −2.78 dB, respectively.

When the power is excited at port ③, the power

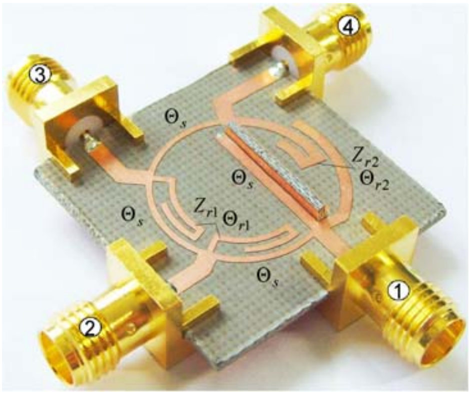

Fig. 15. A fabricated microstrip ring hybrid.

Table 9. Fabrication data for a microstrip compact wideband coupled-line ring hybrid.

$\Theta_s = 55°$, $Z_s = 86.3\ \Omega$, $Z_{0e}^s = 64.21\ \Omega$, $Z_{0o}^s = 25.8\ \Omega$, ($Z_{r1} = 86.4\ \Omega, \Theta_{r1} = 54.5°$), ($Z_{r2} = 63.85\ \Omega, \Theta_{r2} = 60°$)	
$Z_s = 86.3\ \Omega$	w =0.58 mm, ℓ =14.5 mm
$Z_{0e}^s = 64.21\ \Omega$	w_e =1.08 mm, ℓ =13.8 mm, s = 0.76 mm
$Z_{0o}^s = 25.8\ \Omega$	Z_v = 43.16 Ω → w_h =1.04 mm, ℓ =13.8 mm
(Z_{r1}, Θ_{r1})	w = 0.577 mm, ℓ = 14.32 mm
(Z_{r2}, Θ_{r2})	w = 1.08 mm, ℓ = 15.4 mm
50 Ω	w = 1.687 mm

division characteristics are measured and plotted in Fig. 16(b) where measured S_{23} and S_{43} at the design center frequency of 2 GHz are −2.8 dB and −3.2 dB, respectively. The measured matching performance is plotted in Fig. 17(a) where the return loss is less than −15 dB in the frequency range of 1.66 GHz to 2.18 GHz. In the proposed compact ring hybrids case, $|S_{11}| = |S_{44}|$, $|S_{22}| = |S_{33}|$, $|S_{13}| = |S_{24}|$ and the measured isolation is also compared in Fig. 17(b) where almost perfect isolation is achieved in more than 20 % fractional bandwidth.

VI. Conclusions

In this paper, two types of wideband ring hybrids

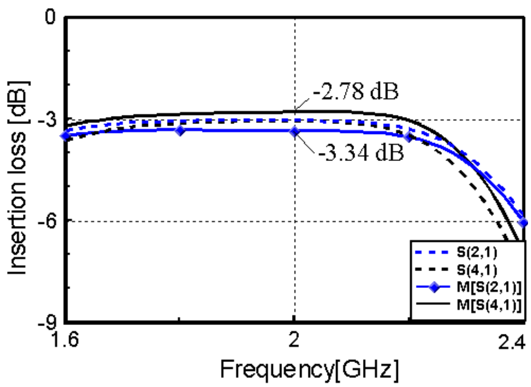

(a) Power division from port ①

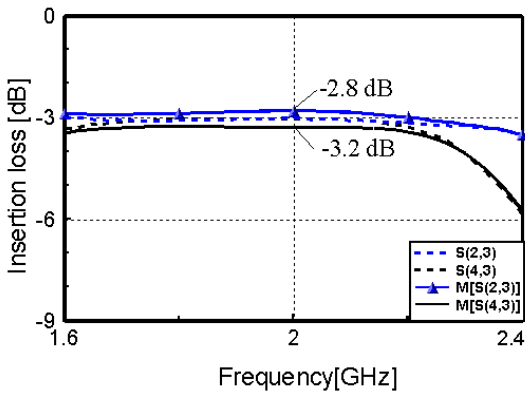

(b) Power division from port ③

Fig. 16. Results measured and predicted are compared.

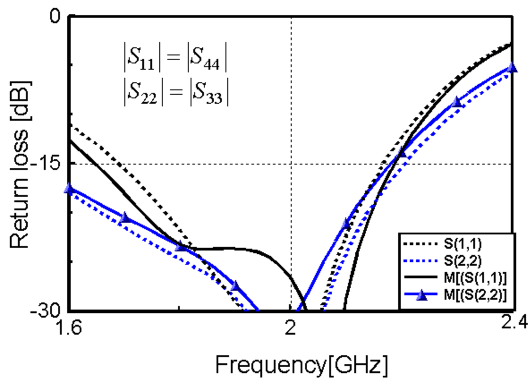

(a) Return loss

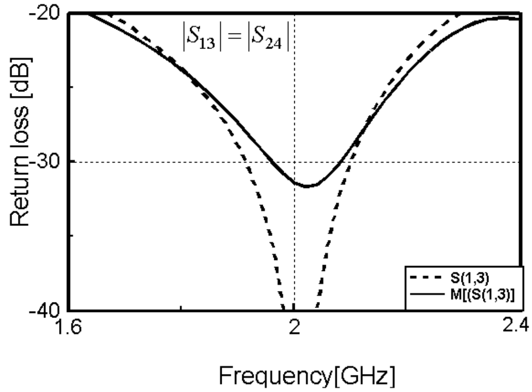

(b) Isolation

Fig. 17. Results measured and predicted are compared.

(one is composed of a set of coupled-line sections and another of a left-handed transmission-line section) were discussed and compared. The compared results showed the coupled-line ring hybrid was better than the left-handed ring hybrid in every point.

However, the coupled-line ring hybrid had a realization problem; perfect matching could be achieved only with -3 dB coupling coefficient. To solve this problem, a set of coupled-line sections with two shorts was synthesized and design equations, with which the coupled-line ring hybrids could be designed without any restriction of coupling power, were derived. Based on the derived design equations, modified Π-type of transmission-line equivalent circuit was newly suggested. The modified one was similar to the conventional one but a set of coupled-line sections was replaced with a transmission-line section. Using the modified transmission-line equivalent circuit, a $3\lambda/4$ transmission-line section of a conventionala ring hybrid could be reduced to less than $\pi/2$ and compact wideband coupled-line ring hybrid was suggested using both modified and conventional ones.

To verify the compact wideband coupled-line ring hybrids, one with the total transmission-line length 160° was compared with a conventional ring hybrid and the compared results showed that the bandwidth of the proposed compact ring hybrid was much wider than that of the conventional one, in spite of being three times smaller in size.

Using the suggested transmission-line equivalent circuit, all the passive components including the ring hybrids can be reduced more. Using the proposed compact wideband coupled-line ring hybrids, all the electrical equipments consisting of ring hybrids can be reduced.

References

[1] W. A. Tyrrel, "Hybrid circuits for microwaves", *Proc. IRE.*, vol. 35, pp. 1294-1306, Nov. 1947.

[2] V. I. Albanese, W. P. Peyser, "An analysis of a broad-band coaxial hybrid ring", *IRE Trans. Microwave Theory Tech.*, vol. 6, pp. 369-373, Oct. 1958.

[3] W. V. Tyminski, A. E. Hylas, "A wide-band hybrid ring for UHF", *Proc. IRE.*, pp. 81-87, Jan. 1953.

[4] S. March, "Wideband stripline hybrid ring", *IEEE Trans. Microwave Theory Tech.*, vol. MTT-16, pp. 361-362, Jun. 1968.

[5] L. K. Yeung, Y. E. Wang, "A novel 180° hybrid using broadside-coupled asymmetric coplanar striplines", *IEEE Trans. Microwave Theory Tech.*, vol. 55, pp. 2625-2630, Dec. 2007.

[6] C. -H. Chi, C. -Y. Chang, "A new class of wideband multiseciton 180° hybrid rings vertically installed planar couplers", *IEEE Trans. Microwave Theory Tech.*, vol. 54 pp. 2478-2486, Jun. 2006.

[7] H. -R. Ahn, Ingo Wolff, and Ik-Soo Chang, "Arbitrary termination impedances, arbitrary power division and small-sized ring hybrids", *IEEE Trans. Microwave Theory Tech.*, vol. 45, pp. 2241-2247, Dec. 1997.

[8] C. -H. Ho, L. Fan, and K. Chang, "Broad-band uniplanar hybrid-ring and branch-line couplers", *IEEE Trans. Microwave Theory Tech.*, vol. 41, pp. 2116-2124, Dec. 1993.

[9] C. -H. Ho, L. Fan, and K. Chang, "Slotline annular ring elements and their applications to resonator, filter and coupler design", *IEEE Trans. Microwave Theory Tech.*, vol. 41, pp. 1648-1650, Sep. 1993.

[10] C. -H. Ho, L. Fan, and K. Chang, "New uniplanar coplanar waveguide hybrid-ring couplers and magic-T's", *IEEE Trans. Microwave Theory Tech.*, vol. 42, pp. 2440-2448, Dec. 1994.

[11] H. Okabe, C. Caloz, and T. Itoh, "A compact enhanced-bandwidth hybrid ring using an artificial lumped-element left-handed transmission line section", *IEEE Trans. Microwave Theory Tech.*, vol. 52, pp. 798-804, Mar. 2004.

[12] L. Fan, C. -H, Ho, S. Kanamaluru, and K. Chang, "Wide-band reduced sized uniplanar magic-T hybrid ring and de Ronde's CPW-slot couplers", *IEEE Trans. Microwave Theory Tech.*, vol. 43, pp. 2749- 2758, Dec. 1995.

[13] B. -H. Murgulescu, E. Moisan, P. Leaude, E. Penard, and I. Zaquine, "New wideband 0.67 λ_g circumference 180° hybrid ring coupler", *Electronic Lett.*, vol. 30, no. 4, pp. 299-300, Feb. 1994.

[14] T. Hirota, A. Minakawa, and M. Muraguchi, "Reduced-size branch-line and rat-race hybrids for uniplanar MMIC's", *IEEE Trans. Microwave Theory Tech.*, vol. 38, pp. 270-275, Mar. 1990.

[15] M. -L. Chung, "Miniaturized ring coupler of arbitrary reduced size", *IEEE. Microwave Component Lett.*, vol. 15, no. 1, pp. 16-18, Jan. 2005.

[16] H. -R. Ahn, *AsymmetrIc Passive Components in Microwave Integrated Circuits*, New York, John Wiley & Sons, Inc., Aug. 2006.

[17] H. -R. Ahn, I. -S. Chang and S. -W. Yun, "Miniaturized 3-dB ring hybrid terminated by arbitrary impedances", *IEEE Trans. Microwave Theory Tech.*, vol. 42, pp. 2216-2241, Dec. 1994.

[18] S. J. Parisi, "180° lumped element hybrid", in *IEEE MTT-S Dig.*, pp. 1243-1246, 1989.

[19] R. K. Gupta, W. J. Gestinger, "Quasi-lumped-element 3- and 4-port networks for MIC an MMIC applications", in *IEEE MTT-S Dig.*, pp. 409-411, 1984.

[20] H. -R. Ahn, B. Kim, "Transmission-line directional couplers for impedance transforming", *IEEE Microwave and Wireless Components Letters*, pp. 537-539, Oct. 2006.

[21] H. -R. Ahn, B. Kim, "Toward integrated circuit size reduction", *IEEE Microwave Magazine*, pp. 65-75, Feb. 2008.

[22] H. -R. Ahn, *Resonators, in Encyclopedia of RF*

and Microwave Engineering, Wiley, 2005.

[23] G. Mathaei, L. Young, and E. M. T. Jones, *Microwave Filters, Impedance-Matching Networks and Coupling Structures*, Artech House, NJ, USA, pp. 36, 1985.

[24] Y. Konishi, I. Awai, Y. Fukuka and M. Nakajima, "A directional coupler of a vertically installed planar circuit structure", *IEEE Trans. Microwave Theory Tech.*, vol. 36, pp. 1057-1063, Jun. 1988.

안 희 란

1988년: 서강대학교 전자공학과 (공학사)
1990년: 서강대학교 전자공학과 (공학석사)
1994년: 서강대학교 전자공학과 (공학박사)
1996년~2002년: 독일 Duisburg-Essen University Habilitation 수료
2003년~2005년: 한국과학기술원 방문교수
2005년~현재: 포항공과대학교 연구교수
Wiley 출판, "Asymmetric passive components in microwave integrated circuit"의 저자
[주 관심분야] 비대칭 수동 소자, Microwave 회로 설계, microwave 의료기기 개발

김 정 준

2007년 2월: 한양대학교 전자공학부 전자공학과 (공학사)
2007년 3월~현재: 포항공과대학교 전자컴퓨터공학부 전자과 석사과정
[주 관심분야] 고효율 고선형성 RF 전력 증폭기 설계

김 범 만

1979년 2월: 카네기 멜론대학 전자공학과 (공학박사)
1978년~1981년: GTE Lab. 연구원
1981년~1988년: TI Central Research Lab. 연구원
1989년~2003년: 포항공과대학교 전자컴퓨터공학부 정교수
1994년~2004년: 포항공과대학교 마이크로웨이브 응용 연구센터(MARC, funded by ADD) 센터장
2002년 7월~2005년 6월: T-MTT Associate Editor(IEEE)
2003년 4월~현재: 포항공과대학교 전자컴퓨터공학부 BK 사업 단장
2003년~2004년: 한국과학기술한림원 종신회원 및 공학부정보통신 분과장
2004년~2005년: 대한전자공학회 협동 부회장
2004년~현재: 포항공과대학교 전자컴퓨터공학부 남고석좌교수
2005년 1월~2007년 12월: Distinguished Lecturer(IEEE MTT society)
2006년~현재: 포항공과대학교 전자컴퓨터공학부 주임교수
2007년 1월~현재: IEEE Fellow 선정
[주 관심분야] 이동통신용 전력 증폭기, RF 회로 설계 및 소자 모델링, III-V 화합물 반도체, 초고주파 집적회로(MMIC) 설계 및 구현, 밀리미터 웨이브 회로 설계